CHARACTERIZING TITAN'S HAZE WITH A BALLOON-BORNE SPECTROPOLARIMETER SPEX

N. Silvestri[1,2], D. M. Stam[1], J. M. Smit[1], and J. H. H. Rietjens[1]

[1]*Earth and Planetary Science Division, SRON Netherlands Institute of Space Research, Sorbonnelaan 2, 3584 CA, Utrecht, The Netherlands*

[2]*Astrodynamics & Space Missions Department, Faculty of Aerospace Engineering, Delft University of Technology, Kluyverweg 1, 2629 HS, Delft, The Netherlands - Email: nicoletta.silvestri@gmail.com, d.m.stam@sron.nl, j.m.smit@sron.nl, j.h.h.rietjens@sron.nl*

ABSTRACT

Saturn's moon Titan has a thick, hazy atmosphere. Knowing the properties of the hazes is crucial for understanding the existence and evolution of this atmosphere and the dynamical processes that take place. We present SPEX, the Spectropolarimeter for Planetary EXploration, as an instrument to retrieve information on the number density, composition, size and shape of the haze particles. As payload on a balloon that floats through Titan's atmosphere, SPEX would measure simultaneously the radiance and degree and direction of linear polarization of sunlight that has been scattered within Titan's atmosphere from 0.4 to 0.8 μm. In particular the degree of linear polarization of the scattered light is known to be very sensitive to the microphysical properties of the scattering particles. We show numerical simulations of radiance and polarization spectra of scattered sunlight and of radiance and polarization spectra as retrieved from the SPEX observations. The spectral resolution of the latter spectra depends on our choice of optical components for SPEX. In particular, in order to resolve the strong spectral features that are due to absorption by methane, the birefringent retarder should have a thickness of 16 mm.

Key words: Titan; aerosol; haze; atmosphere; balloon; spectropolarimetry.

1. INTRODUCTION

It has been known since the flybys of the Voyagers that Titan's atmosphere contains thick haze layers. The haze particles are most probably composed of various types of hydrocarbons which might be a sink for methane and its by-products [3, 4], and are thought to have fractal-like shapes [13, 17, 14]. Knowledge on the number density, the microphysical properties (size, shape, and composition) of the haze particles and the spatial and temporal variations therein is key to understanding the radiative, chemical and dynamical processes that take place in this unique atmosphere. Such knowledge can be obtained by measuring and analyzing the radiance and the state (i.e. the degree and direction) of polarization of sunlight that has been scattered by the haze particles. In particular the degree of (linear) polarization is known to be very sensitive to the particles' microphysical properties [1].

In the past decades there have been several planetary missions that carried instruments with polarimetric capabilities to study planetary atmospheres. Examples are Pioneers 10 and 11, Voyager 1 and 2, Pioneer Venus, the Galileo mission, and both the Saturn orbiter and the Huygens probe of the Cassini mission. The polarimetry with these instruments was and is based on measurements of the radiance of the scattered sunlight through polarisation filters in two or three positions (see Eqs. 1.5 and 1.6 of [1]). From combining these separate radiance measurements, the total radiance, the degree and direction of linear polarization can be obtained. The disadvantage of this polarimetric technique is that the separate radiance measurements are not performed simultaneously, and usually through different optical systems (e.g. different polarization filters). As a result, the degree of polarization that is hence obtained can have an error of several percent, which is too large to use polarimetry to its full potential. In addition, the polarimetry on previous and current planetary missions was and is limited to broadband measurements, while the degree of linear polarization shows at least as much spectral features as the radiance [2].

The SPEX instrument (Spectropolarimeter for Planetary EXploration) that we present in this paper, uses a novel polarimetric technique to simultaneously measure the radiance, the degree and the direction of linear polarization of scattered sunlight across the wavelength region from 0.4 to 0.8 μm, with the spectral resolution of the measured radiance spectra of about 2 nm, and that of the polarization spectra somewhat larger [5].

The SPEX instrument can be placed on an orbiter to measure the radiance and state of polarization of sunlight that has been reflected by Titan. This reflected sunlight will mainly contain information on Titan's outer haze layers. Here, we focus on a SPEX as payload for a bal-

loon that floats through the Titan atmosphere as proposed to ESA's Cosmic Vision Programme in the Titan Saturn System Mission (TSSM) proposal [20]. This hot-air balloon would float at an altitude of about 10 km, below the lowest haze layer. SPEX as payload of this balloon would measure the radiance and state of polarization of sunlight that is scattered and transmitted through the haze layers.

SPEX on a balloon would not be the first polarimeter investigating Titan's atmosphere from the inside. The Descent Imager/Spectral Radiometer (DISR) [16] on the Huygens probe also performed polarimetric measurements and obtained valuable information on the shape and size of the aerosols at Huygens landing site [17]. The DISR instrument used two orthogonal polarization filters in combination with a blue and a red filter, thus four separate radiance measurements to determine the radiance and degree of polarization of the scattered sunlight and their broadband spectral variation. The errors resulting from the time differences and the differences in the optical properties of the filters (apart from the error in the polarization due to using only two instead of three radiance measurements per wavelength) will affect the retrieval of the microphysical properties of the haze particles. [1] Since SPEX would be able to measure the scattered radiance and the (complete) state of polarization simultaneously and continuously from 0.4 to 0.8 μm, and of course because it would float through the atmosphere as part of the balloon payload, it could add tremendously to our knowledge on Titan's haze particles.

This paper is structured as follows. In Sect. 2, we define the radiance and state of polarization as measured by SPEX. In Sect. 3, we describe the radiative transfer algorithm and the model planets that we use for our numerical simulations of scattered sunlight, and results of these simulations. In Sect. 4, we describe SPEX and explain its novel polarimetric technique, and present simulated SPEX observations. In Sect. 5, we discuss the adaptations of a SPEX instrument that was designed for a Mars mission to a Titan mission. Section 6 finally, contains the conclusions.

2. RADIANCES AND POLARIZATION

We describe the radiance and state of polarization of a beam of radiation by a Stokes vector **I** [6, 7], as follows

$$\mathbf{I}(\lambda) = \begin{bmatrix} I(\lambda) \\ Q(\lambda) \\ U(\lambda) \\ V(\lambda) \end{bmatrix}, \tag{1}$$

with λ the wavelength of the radiation, I the total radiance of the beam, Q and U representing the linearly polarized, and V the circularly polarized radiance. All Stokes parameters have the dimension of W m^{-2} sr^{-1} μm^{-1}. Stokes parameters Q and U are defined with respect to a reference plane [1, 8]. For the simulations of light that has been singly scattered by a sample of aerosol particles, we will use the scattering plane, which contains both the direction of the incoming and that of the scattered beam of radiation, as the reference plane. For the simulations of sunlight that has been scattered in Titan's atmosphere, we will use the local meridian plane, which contains both the direction towards the zenith and the direction of propagation of the scattered light.

We define the degree of polarization of the beam of radiation as follows:

$$P(\lambda) = \frac{\sqrt{Q^2(\lambda) + U^2(\lambda) + V^2(\lambda)}}{I(\lambda)}. \tag{2}$$

In planetary atmospheres, the circularly polarized radiance V is usually very small [1]. We will neglect V, and assume P is the degree of linear polarization of the sunlight that is scattered in Titan's atmosphere:

$$P(\lambda) = \frac{\sqrt{Q^2(\lambda) + U^2(\lambda)}}{I(\lambda)}. \tag{3}$$

For incident unpolarized light that has been singly scattered by a sample of aerosol particles, U equals zero, and we will use the following definition of the degree of polarization that includes information on the polarization direction

$$P_{\rm S} = -\frac{Q}{I}. \tag{4}$$

If $P_{\rm S}$ is positive (negative), the light is polarized perpendicular (parallel) to the scattering plane.

For the sunlight that has been scattered in Titan's atmosphere, the direction of (linear) polarization with respect to the reference plane is represented by the angle:

$$\chi(\lambda) = \frac{1}{2} \arctan \frac{U(\lambda)}{Q(\lambda)}, \tag{5}$$

where the value of χ that should be chosen is the one which makes $\cos 2\chi$ have the same sign as Q [1]. When $\chi = 90^\circ$ ($\chi = 0^\circ$), the direction of polarization is perpendicular (parallel) to the reference plane.

From SPEX measurements, we can derive the total radiance I, the degree of linear polarization P, and the direction of polarization χ of light, as functions of λ. Note that in order to derive the absolute total radiance, we will have to calibrate SPEX, e.g. by using an internal reference light source. No such calibration is required for deriving P and χ, since these are relative measures.

3. CALCULATING SCATTERED SUNLIGHT

3.1. Our radiative transfer algorithm

For our numerical simulations of sunlight that is scattered in Titan's atmosphere, we use an adding-doubling algo-

[1] Using two instead of three polarization filters can in principle be accounted for in the radiative transfer calculations in the retrieval, but the missing information will limit the accuracy of the retrievals.

rithm that fully includes multiple scattering and polarization [8, 9]. The algorithm is monochromatic, i.e. every wavelength is treated separately.

The algorithm (for details of the calculations, see [8]) assumes a model atmosphere that consists of a stack of horizontally homogeneous layers that can differ from each other, and that is bounded below by a horizontally homogeneous surface. The surface reflects Lambertian (i.e. isotropic and completely depolarizing) with a (wavelength dependent) albedo $A_{\rm S}$. Each atmospheric layer contains gaseous molecules and, optionally, aerosol particles. For each layer, we have to specify for each type of particles, their column number density (in $\rm m^{-2}$), and for each wavelength λ, their extinction cross-section σ, single scattering albedo $\tilde{\omega}$ and single scattering matrix $\mathbf{F}$.

The (total) optical thickness of a layer due to a certain type of particles and at a given wavelength is calculated by multiplying the column number density of the particles with their extinction cross-section at the given wavelength. The optical thickness b of a layer is thus given by

$$\begin{aligned} b(\lambda) &= b_{\rm m}(\lambda) + b_{\rm a}(\lambda) \\ &= b_{\rm msca}(\lambda) + b_{\rm mabs}(\lambda) + b_{\rm asca}(\lambda) + b_{\rm aabs}(\lambda), \end{aligned} \tag{6}$$

with $b_{\rm m}$ and $b_{\rm a}$ the optical thicknesses of the gases and the aerosol particles, respectively, which are the sums of the scattering and the absorption optical thicknesses of the gases and the aerosol particles, $b_{\rm msca}$, $b_{\rm mabs}$, $b_{\rm asca}$, and $b_{\rm aabs}$, respectively. Obviously, $b_{\rm msca} = \tilde{\omega}_{\rm m}\ b_{\rm m}$, and $b_{\rm asca} = \tilde{\omega}_{\rm a}\ b_{\rm a}$. The single scattering albedo $\tilde{\omega}$ of the mixture of gases and particles in a layer is given by

$$\tilde{\omega}(\lambda) = \frac{b_{\rm msca}(\lambda) + b_{\rm asca}(\lambda)}{b_{\rm m}(\lambda) + b_{\rm a}(\lambda)}. \tag{7}$$

The single scattering matrix $\mathbf{F}$ of the gases and particles in a layer is given by

$$\mathbf{F}(\Theta, \lambda) = \frac{b_{\rm msca}(\lambda)\mathbf{F}_{\rm m}(\Theta, \lambda) + b_{\rm asca}(\lambda)\mathbf{F}_{\rm a}(\Theta, \lambda)}{b_{\rm msca}(\lambda) + b_{\rm asca}(\lambda)} \tag{8}$$

where Θ is the single scattering angle ($0^\circ \leq \Theta \leq 180^\circ$, $\Theta = 0^\circ$ implies forward scattering), and $\mathbf{F}_{\rm m}$ and $\mathbf{F}_{\rm a}$ are the single scattering matrices of the gaseous molecules and the aerosol particles, respectively [8]. Each scattering matrix is normalized such that the average of the single scattering phase function, i.e. element F_{11} of each matrix, over all scattering angles equals one, as follows

$$\frac{1}{4}\int_0^{4\pi} F_{11}(\Theta, \lambda) d\Omega = 1, \tag{9}$$

where $d\Omega$ is an element of solid angle. If incident light is unpolarized, the degree of linear polarization of the light that is singly scattered by the gases and particles can be written as $P_{\rm S} = -F_{12}/F_{11}$ (cf. Eq. 4).

Apart from the properties of the surface and atmosphere, the radiative transfer depends on the illumination and viewing geometries. We specify the solar zenith angle θ_0 (the angle between the direction towards the sun and the upward vertical), the instrument zenith viewing angle θ (the angle between the direction of propagation of the observed light and the downward vertical), and the azimuthal angles ϕ_0 and ϕ that are measured between an arbitrary vertical plane and the directions of propagation of, respectively, the incoming and observed beams of radiation. Since our model atmosphere and surface are horizontally homogeneous, only $\phi - \phi_0$ is relevant. When $\phi - \phi_0 = 0^\circ$, the instrument is looking in the direction towards the sun. When $\phi - \phi_0 = 180^\circ$, it has the sun 'in its back.'

Since we assume that SPEX will be payload on a balloon floating below Titan's lowest haze layer, it will observe sunlight that has been transmitted through the atmosphere. With our adding-doubling algorithm, we calculate the transmission matrix $\mathbf{T}$ of the atmosphere-surface system, and obtain the Stokes vector of the transmitted light using [1]

$$\mathbf{I}(\lambda, \theta_0, \theta, \phi - \phi_0) = \cos\theta_0 \mathbf{T}(\lambda, \theta_0, \theta, \phi - \phi_0)\mathbf{F}_0(\lambda), \tag{10}$$

where $\mathbf{F}_0$ is the Stokes vector of the incoming solar radiation, with πF_0 the solar flux at the top of the atmosphere, measured perpendicularly to the direction of incidence. The solar radiation is assumed to be unidirectional and unpolarized, and is thus given by $\mathbf{F}_0 = F_0\mathbf{1}$, with $\mathbf{1}$ the unit column vector. Note that P and χ of the scattered sunlight are independent of F_0.

3.2. The model atmosphere and surface

To describe the reflection of sunlight by Titan's surface, we use a surface albedo equal to 0.04, which is representative for Titan's dark terrain [12].

We model Titan's atmosphere from 0 km to 400 km with 34 layers. We calculate the molecular scattering optical thickness $b_{\rm msca}$ of each layer as described in [8], using the values of [10] for the ambient pressure and temperature at the bottom and top of each layer. Across SPEX' wavelength region, the main gaseous absorption bands are due to methane. We calculate the molecular absorption optical thickness $b_{\rm mabs}$ of each layer as described in [8], using the methane mixing ratio profile from [19] and the methane absorption coefficients from [18].

Apart from gaseous molecules, each atmospheric layer also contains haze aerosol particles. For the simulations presented in this paper, we use the same type of aerosol throughout the atmosphere. We assume that the aerosol optical thickness $b_{\rm a}$ varies with altitude as described by [17], with the total atmospheric $b_{\rm a}$ at λ =550 nm, equal to 8.10. The cumulative $b_{\rm a}$ at $\lambda = 550$ nm as a function of altitude is shown in Fig.1.

The actual wavelength dependence of $b_{\rm a}$, as well as $\tilde{\omega}_{\rm a}$ and $\mathbf{F}_{\rm a}$ of the aerosol particles depends on the particles' microphysical properties (size, shape, composition). We

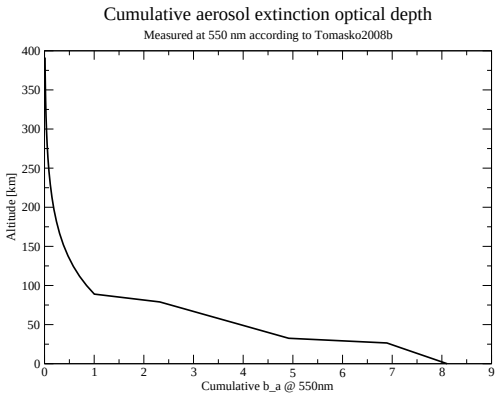

Figure 1. The cumulative optical thickness of the haze aerosol in our model atmosphere as a function of the altitude at $\lambda = 550$ nm (from [17]).

assume aggregate, fractal-type particles that consist of clusters of spherical monomers. In our simulations, we consider particles that formed through Ballistic Particle-Cluster Aggregation (BPCA), and particles that formed through Diffusion-Limited Aggregation (DLA). The difference between the two aggregation processes is that with ballistic aggregation, the monomers move along straight lines before colliding with the aggregate, while with the diffusion limited aggregation, the monomers are subject to Brownian motions. According to [13], BPCA should be more common in the higher, thinner layers of the atmosphere, while DLA is more appropriate for the lower, denser layers.

We calculated the optical properties of the two types of fractal aerosol particles across SPEX' wavelength region using the 3-D positions of the monomers provided by dr. Y.V. Skorov [13] as input for the super-position T-matrix code [15], adopting the refractive index values of [11]. Both our BPCA and our DLA particles consist of 256 monomers, with the monomer's radius equal to 0.05 μm in accordance with [14]. We combined the calculated optical properties of the aggregate particles and their mirror particles. Including the mirror particles removed the negative branch of polarization that [13] found in their single scattering simulations and that did not agree with the DISR observations.

Figure 2 illustrates the shapes of the fractal-type aerosol particles that we used in our model atmosphere. The BPCA-particle is characterized by a compact core that is surrounded by 'arms' of monomers. The DLA-particle lacks the extended arms of monomers. The different shapes of the two types of particles yield different scattering behaviours. In Fig. 3 we show the calculated [15] phase functions and degree of linear polarization $P_{\rm S}$ of unpolarized incident light that is singly scattered by the two types of particles for $\lambda = 0.47$ μm and $\lambda = 0.83$ μm, respectively.

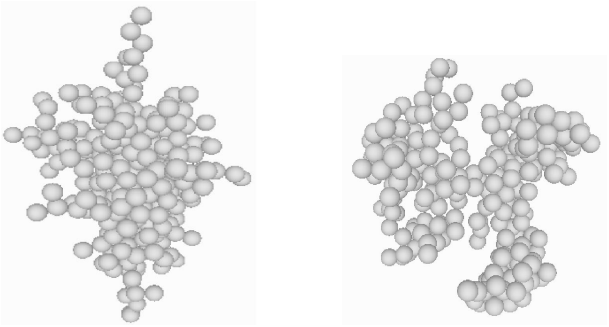

Figure 2. Graphs illustrating the structure of the BPCA-particles (on the left) and the DLA-particles (on the right). Both particle types consist of 256 monomers.

The phase functions for both types of particles clearly show forward scattering behaviour (see Fig. 3). The strength of the forward scattering peak is significantly stronger for both types of particles for the shorter wavelength ($\lambda = 0.47$ μm). With the shorter wavelength, the phase functions for both types of particles also show more angular features. These angular features are much less obvious for $\lambda = 0.83$ μm. Such features are usually due to interference between light that has been scattered by different, similarly sized particles [1]. Apparently, when the light has a short wavelength compared to the fractal particles, the light scattered by the different monomers that make up the fractal particle will interfere and give rise to the angular features [23]. With increasing λ, the light will increasingly be scattered by the fractal particle as a whole, and the interference patterns disappear due to the different scales of the macroscopic particle. Since the DLA-particle is more compact and thus somewhat smaller than the BPCA-particle, its phase function is the more symmetric one at $\lambda = 0.83$ μm.

The degree of linear polarization $P_{\rm S}$ of the light that is singly scattered by the two types of particles (see Fig. 3) shows the bell-shape that is characteristic for light that is scattered by particles that are small with respect to the wavelength [1]. Apparently, this polarization signal is dominated by that of light that is scattered by the monomers. An effect of the macroscopic shape of the particles on $P_{\rm S}$ is found in the strength of the maximum of the polarization curve: with increasing λ, the maximum $P_{\rm S}$ increases more for the compact DLA-particles than for the fluffier BCPA-particles.

3.3. Sunlight that is scattered in Titan's atmosphere

Here, we present results of numerical simulations of the radiance I (Eq. 10) and degree of linear polarization P (Eq. 3) of sunlight that has been scattered in Titan's atmosphere and that emerges at the bottom of the atmosphere. We'll show spectra for different amounts of aerosol particles, for different illumination and viewing geometries, and for the two types of particles. We assume that the incoming solar flux equals π, i.e. $F_0 = 1$ in Eq. 10. In our

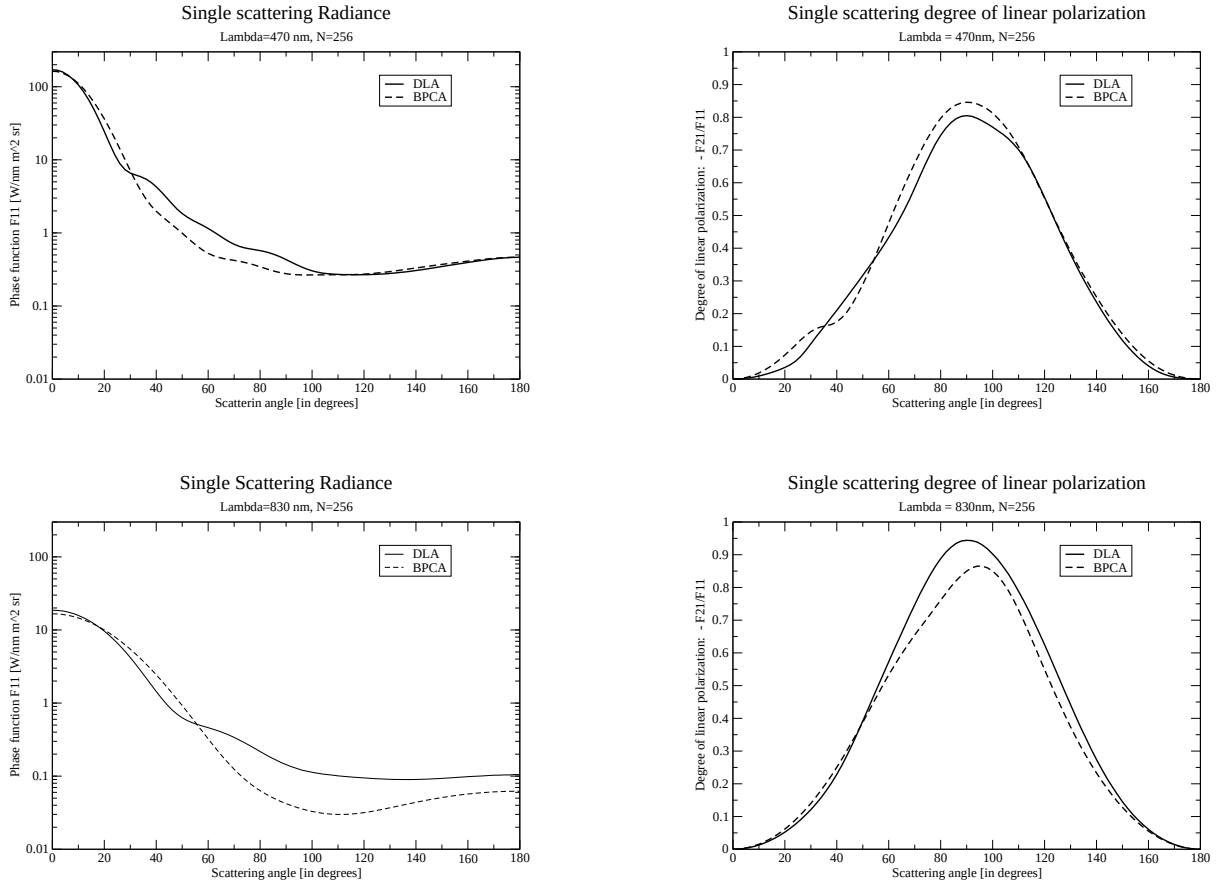

Figure 3. The phase function (left) and degree of linear polarization $P_{\rm S}$ (right) of unpolarized incident light that is singly scattered by the BPCA-particles (dashed lines) and the DLA-particles (solid lines) as functions of the single scattering angle Θ, for $\lambda = 0.47$ μm (top) and $\lambda = 0.87$ μm (bottom).

discussion of the results, we will focus on the continuum radiances and polarization.

Figure 4 shows I and P as functions of the wavelength λ from 0.3 to 0.9 μm (SPEX' spectral range is somewhat shorter, namely from 0.4 to 0.8 μm). The solar zenith angle θ_0 is 0° (the sun is thus in the zenith), and the viewing angle θ ranges from 0° (looking towards the zenith) to 60°. For $\theta_0 = 0^\circ$, the azimuthal angle $\phi - \phi_0$ is undefined. The aerosol optical thickness profile as shown in Fig. 1 is used, with a total optical thickness of 8.1 at $\lambda = 0.55$ μm, and the aerosol particles are of the DLA-type.

As can be seen in Fig. 4, the scattered radiance spectra show strong absorption lines that are due to the methane in the atmosphere. With increasing λ, the continuum radiance of each spectrum increases steadily because of the decrease of the atmospheric optical thickness (gas + aerosol). The continuum radiance is highest for $\theta = 0^\circ$ and decreases with increasing θ, because of the forward scattering behaviour of the phase function of the aerosol particles (see Fig. 3), and because of the increase of the effective atmospheric optical thickness with increasing θ (the sun is in the zenith).

The scattered polarization spectra (Fig. 4) can, like the radiance spectra, be thought of as to consist of a continuum with super-imposed spectral features that are due to absorption of light by methane. The continuum degree of polarization is small at the smallest wavelengths, because at those wavelengths, the optical thickness b of the atmosphere is relatively large. The multiple scattering of light in an optically thick atmosphere will usually decrease P. With increasing λ, b decreases, the multiple scattering decreases, and the continuum P increases. The continuum P will also depend on the single scattering $P_{\rm S}$ of the gas molecules and aerosol particles in the atmosphere. For example, at the longest wavelengths, P will be mostly determined by low order scattering by aerosol particles. The values of the continuum P at $\lambda = 0.9$ μm for each value of θ compare very well with those in Fig. 3 for the corresponding single scattering values of Θ (i.e. $\theta_0 = 0^\circ$ and $\theta = 60^\circ$ correspond to $\Theta = 60^\circ$).

From $\lambda \approx 0.4$ to 0.5 μm, the continuum P is low for all values of θ. This is called a 'neutral' point of polarization, and it is due to interference of the polarization signatures

of single and second or higher order scattered light. In the methane absorption bands, P generally increases with increasing absorption band strength. This is explained by a decrease of multiple scattering with increasing absorption, and hence an increase of P. However, to fully explain the changing shape of P across gaseous absorption bands, one also has to take into account the single scattering properties of the atmospheric molecules and aerosol particles. In the different parts of the absorption band, the transmitted light has been scattered in different regions of the atmosphere, and will carry the polarization signature of the mixture of aerosol particles and gases in those regions.

Figure 5 is similar to Fig. 4, except that the model atmosphere contains twice the amount of aerosol particles (the vertical profile has the same shape). Comparing the radiance spectra in Figs. 5 and 4, we see that doubling $b_{\rm a}$ leaves the general shape of the radiance spectra untouched, while it lowers the absolute radiance values across the continuum for $\theta = 0^\circ$ and 20°, and increases the absolute radiance values across the continuum for $\theta = 40^\circ$ and 60°. Apparently, increasing $b_{\rm a}$ from 8.1 to 16.2 (at $\lambda = 0.55$ μm), makes the sky brightness more homogeneous.

The polarization spectra in Fig. 5 are very similar in shape to those in Fig. 4, except that at the longer wavelengths, doubling $b_{\rm a}$ has led to a significant decrease of the continuum P, which is due to an increase of multiple scattering. At the shorter wavelengths, the amount of multiple scattering hasn't changed much and P seems rather insensitive to the doubling of $b_{\rm a}$ from 8.1 to 16.2 (at $\lambda = 0.55$ μm), probably because scattering of light by the gas molecules is the most important process at those wavelengths. Interestingly, the neutral points of polarization seem to have shifted towards longer wavelengths with the increase of $b_{\rm a}$.

Figure 6 is similar to Fig. 4, except that the solar zenith angle θ_0 is 30° and 60°, respectively. The azimuthal angle $\phi - \phi_0 = 0^\circ$. For $\theta_0 = 30^\circ$, the viewing angles $\theta = 20^\circ$ and 40° are close (10°) to looking into the direction of the sun, which results in a large continuum radiance at the longest wavelengths, where the forward scattering by the aerosol particles is important. At the longest wavelengths and for $\theta = 60^\circ$, the scattered continuum radiance is larger than for $\theta = 0^\circ$, which means that in the red, the horizon is brighter than the zenith sky. At the shortest wavelengths, where scattering by gas molecules is most important, the horizon ($\theta = 60^\circ$) is darker than the zenith sky. For $\theta_0 = 60^\circ$, the viewing angle of 60° is looking straight into the direction of the sun. At the longest wavelengths, the forward scattering by aerosols makes this direction of the sky very bright (note that the spectra only include the scattered light), while the zenith sky is darkest. At the shortest wavelengths, the direction towards the sun is darkest.

The continuum P for $\theta_0 = 30^\circ$ looks very different from that when $\theta_0 = 0^\circ$. In particular, the viewing directions $\theta = 20^\circ$ and 40°, which are closest to looking directly into the sun yield very low degrees of polarization ($< 2\%$), because this is mostly forward scattered light which has a low degree of polarization (see Fig. 3). The curves for $\theta = 0^\circ$ and 60° pertain to similar single scattering angles (i.e. 30°), yet their shapes are quite different because of the interplay between the degree of polarization of singly scattered light at $\Theta = 30^\circ$ and the ratio of single to multiple scattering. The latter depends strongly on the effective atmospheric optical thickness, which increases with the viewing angle. In particular, for $\theta = 60^\circ$, this results in a broad region where P is about zero (a neutral point), which is absent for $\theta = 0^\circ$. For $\theta_0 = 60^\circ$ (Fig. 6), this low degree of polarization is seen for $\theta = 60^\circ$, while for $\theta = 40^\circ$, which is close towards the direction of the sun, the continuum P is low, too.

Figures 7 and 8 show the effects having BPCA instead of DLA-particles, with the same aerosol optical thickness at 0.55 μm, on the transmitted radiance and degree of polarization. The solar zenith angle is 0° (Fig. 7) or 60° (Fig. 8) and results are shown for $\theta = 0^\circ$ and 60° (with $\phi - \phi_0 = 0^\circ$). As can be seen from the radiance spectra in Fig. 7, the DLA-particles show a stronger forward scattering behaviour than the BPCA-particles. For the polarization, and $\theta = 60^\circ$, we see in Fig. 7 that at the shorter wavelengths, there is little difference between DLA and BPCA, while at the longer wavelengths, there is a large difference (just like we would expect based on Fig. 3). With the sun at 60° (Fig. 8), we can again see the single scattering polarization features (Fig. 3) back in the multiple scattering behaviour. In this geometry, both the DLA- and the BPCA-particles give rise to neutral points at certain wavelengths, especially the DLA-particles. What permits to discern the two spectra, is the location of the neutral points. In Fig.8 for a viewing zenith angle of 60°, the DLA-particle presents neutral points at $\lambda \approx 0.8$ μm that the BPCA-particle does not show. The DLA-particles also give rise to inverted polarization in some of the methane absorption bands.

From the spectra we showed, it is clear that the spectral dependence of the degree of linear polarization of sunlight that is transmitted through Titan's atmosphere shows a stronger variation on the particle-type, than the radiance of this light. The latter does show variations, but the general shape of the spectra remains the same, while the continuum radiance is very dependent on the aerosol optical thickness and would thus not constrain particle type [21]. Obviously, preferably, both the radiance and the polarization are measured.

4. THE SPEX INSTRUMENT

4.1. SPEX' novel spectropolarimetric method

In planetary observations, linear polarimetry of a beam of radiation is traditionally done by measuring the beam's radiance in three different polarization directions, e.g. through a single rotatable polarization filter, or through

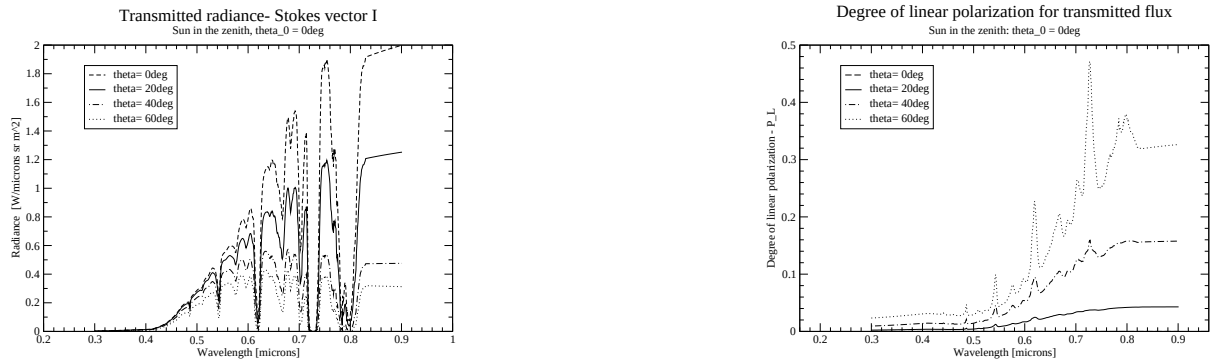

Figure 4. Numerically calculated radiance (on the left) and polarization (right) spectra of sunlight that is scattered in and transmitted through Titan's atmosphere. The solar zenith angle $\theta_0 = 0^\circ$, and the viewing zenith angles are: 0° (solid lines), 20° (dashed lines), 40° (dot-dashed lines), and 60° (dotted lines). Note that for $\theta = 0^\circ$, P equals zero at all wavelengths. The aerosol profile is as shown in Fig. 1 and the aerosol particles are of the DLA-type.

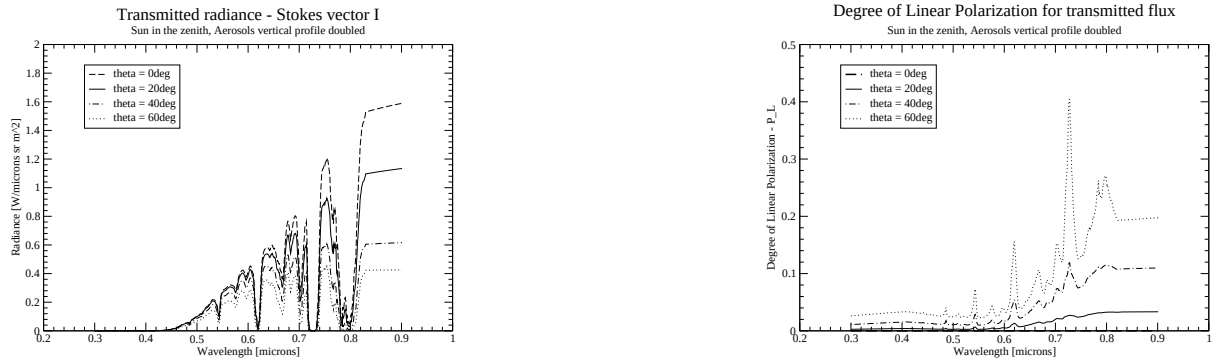

Figure 5. Similar to Fig. 4, except for twice the amount of aerosol particles.

three polarization filters with different orientation angles in a filter wheel. The three radiance measurements are combined to yield the beam's total radiance I, and the linearly polarized radiances Q and U (see [1]). Note that DISR measured only two linearly polarized radiances, hence it could only provide a partial degree of linear polarization, for example, only Q/I, instead of $\sqrt{Q^2+U^2}/I$ (Eq. 3). The main disadvantages of these traditional polarimetric methods are 1. time differences, hence differences in observed scenes and illumination geometries, between the separate radiance measurements, which can cause errors of several percent in the derived degree of polarization, and/or 2. differences in the optical properties of the optical systems, e.g. filters, through which the separate radiance observations are done. In addition, most traditional polarimeters use rotating filters or filter wheels, which carry the risk of getting stuck, while polarimeters that have three (sometimes two) inert optical systems for the radiance measurements are too heavy for a planetary mission (an example is the APS polarimeter on NASA's Earth observing Glory mission that will be launched at the end of this year).

SPEX uses a novel spectropolarimetric technique which allows simultaneous measurements of the total radiance I, and the degree P and direction χ of polarization from 0.4 to 0.8 μm with a spectral resolution of 2 nm for the radiance to slightly larger for the polarization, without moving parts. In addition to being robust, SPEX is small ($<$ 5 kg) and uses little power. Details on SPEX' polarimetric technique can be found in [5]. Here, we will summarize the main characteristics of the technique.

SPEX' spectropolarimetric technique is based on spectral modulation: the radiance spectrum is sinusoidally modulated by the degree and direction of linear polarization of the incoming radiation. The modulation is achieved by a carefully selected series of (passive) optical components. When leaving this pre-optics, the beam of light has been spectrally modulated and continues towards a spectrometer, where an off-the-shelf detector records the modulated spectrum with a 2 nm spectral resolution. The pre-optics consists of an achromatic quarter-wave plate, an athermal multiple-order retarder, and a polarizing beam-splitter, the effects of which we will explain below.

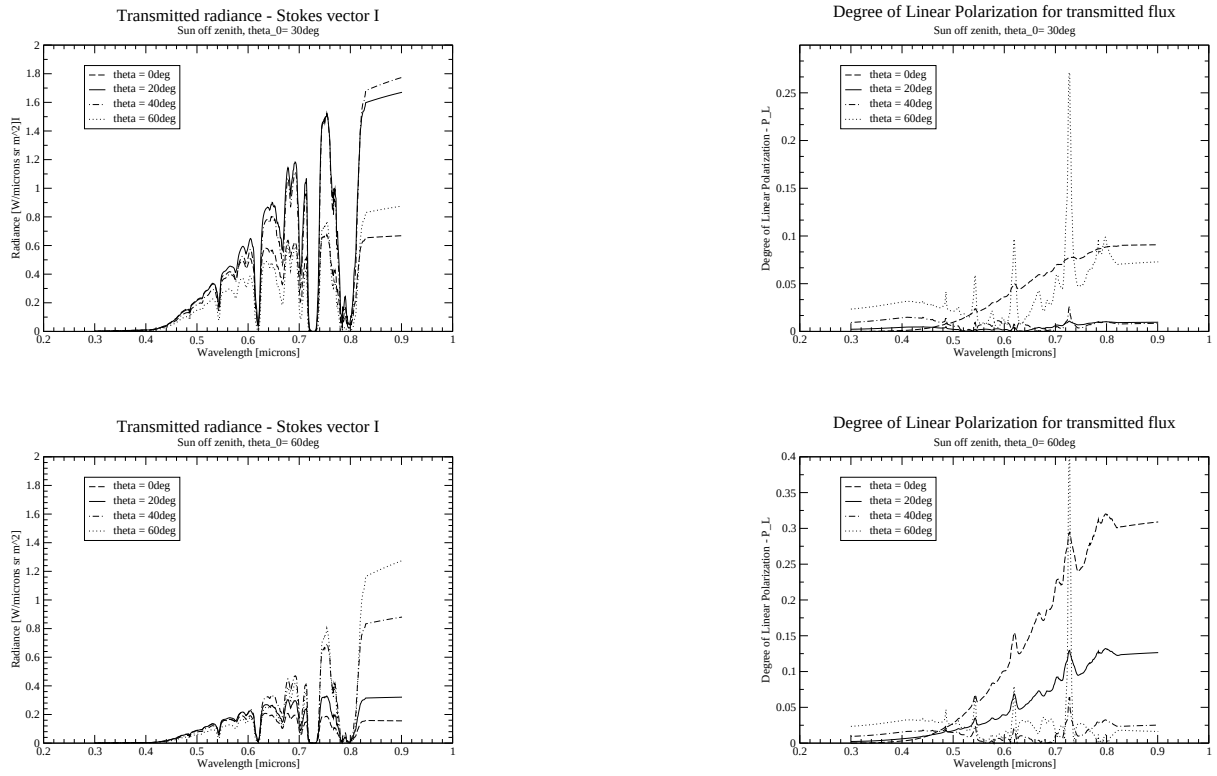

Figure 6. Similar to Fig. 4, except for $\theta_0 = 30°$ (top) and 60° (bottom) instead of 0°. The azimuthal angle $\phi - \phi_0 = 0°$.

1. The achromatic quarter-wave plate
This element has its optical axes oriented such (at 0° and 90°) that Stokes parameter Q passes untouched, while parameter U is converted into circular polarization V (we assume that the light that enters the instrument has $V = 0$). We have chosen a Fresnel rhomb as SPEX' achromatic quarter-wave plate.

2. The athermal multiple-order retarder
This element is the core of the SPEX instrument. A retarder induces a phase difference between two polarization components of a beam of light due to the fact that its indices of refraction have different values for different polarization directions (this is called 'birefringence'). The retarder changes the ellipticity of the light that is incident on it, depending on the wavelength of the light, since the retardance is very achromatic. As an example, light with a wavelength independent degree of linear polarization that is incident on the retarder will leave the optical element with a state of polarization that varies between linear to circular as a function of the wavelength. The axes of our retarder are at 45° and 135°. It consists of MgF_2-Al_2O_3, which has been chosen because its retardance is insensitive to temperature changes.

3. The polarizing beam-splitter
A Wollaston prism is used as a polarizing beam-splitter to filter two orthogonal directions of linear polarized light out of the beam of light that leaves the retarder. Both of the filtered beams have a modulated radiance spectrum with a phase difference of π between them. The modulation is described by the following equations [5]

$$S_{\pm}(\lambda) = \frac{1}{2} S_0(\lambda) \left[1 \pm P(\lambda) \cos \phi(\lambda)\right], \qquad (11)$$

where the phase is given by

$$\phi(\lambda) = \frac{2\pi\delta(\lambda)}{\lambda} + 2\chi(\lambda), \qquad (12)$$

with δ the retardance of the multiple-order retarder (in m), and χ the angle of polarization. In Eq. 11, S_0 is the incoming (unmodulated) radiance spectrum, P the degree of linear polarization of the incoming light, and $S_{\pm}$ the detected (modulated) radiance spectrum with either a 'positive' modulation (indicated by the + sign) or a 'negative' modulation (with the - sign). With SPEX, we detect both the S_+ and the S_- spectrum, and it is clear that by adding these two modulated spectra, the incoming radiance spectrum S_0 is obtained with the spectral resolution with which $S_{\pm}$ are measured. The degree of linear polarization P and the direction of polarization χ can be derived from each of the modulated radiance spectra, using a demodulation algorithm. The spectral resolution of P and χ is on the order of the modulation, which depends on the choice of optical elements, in particular, for a given material of the retarder, on the length of the multiple-order retarder.

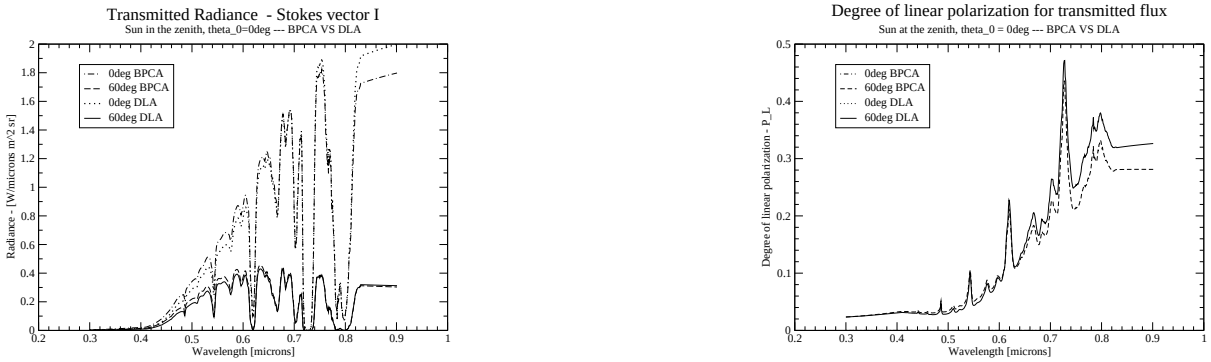

Figure 7. Similar to Fig. 4, except only for the viewing angles $\theta = 0°$ and 60°, and it also includes curves for BPCA-particles instead of DLA-particles (b_a at 0.55 μm is 8.1 for both aerosol types). Note that at $\theta = 0°$, $P = 0$ at all the wavelengths for both BPCA-particle and DLA-particle (see Fig.4).

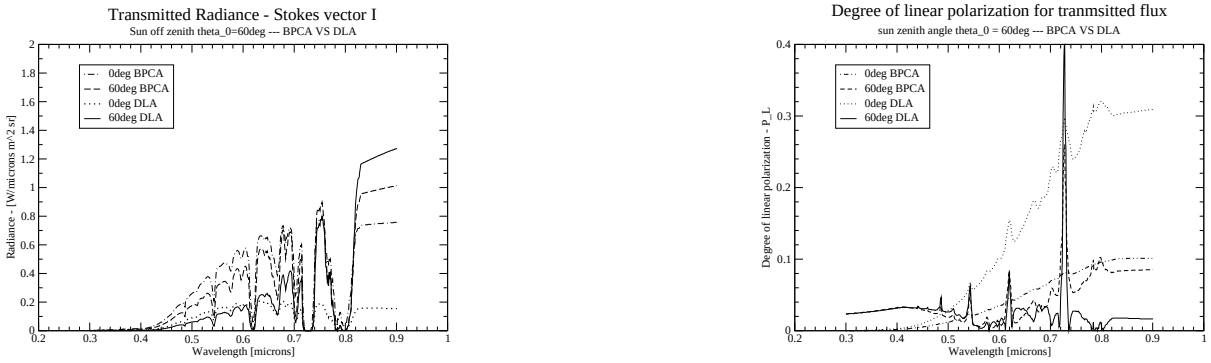

Figure 8. Same as for Fig.7, except for $\theta_0 = 60°$.

4.2. SPEX end-to-end simulator

The SPEX end-to-end simulator is a software tool that fully describes the SPEX instrument, its measurements, and the data analysis for missions to different planets. This tool (which is still under development) facilitates defining the science and instrument requirements, assessing the instrument performance, optimizing calibration routines and tracing potential system degradations during a mission.

The input of the simulator are high-spectral resolution spectra of I, Q, and U (and possibly V), such as those calculated with our adding-doubling radiative transfer algorithm (see Sect. 4). Each optical component of the instrument is modeled using appropriate Mueller matrices including wavelength dependent optical properties of the materials and field-of-view variations of the incident spectra. The modulated spectra at the end of the optical train are imaged on the focal plane array of the detector and binned. A wavelength dependent quantum efficiency, dark-current, read-, shot- and ADC-noise, are included in the calculation, while pixel-to-pixel variations in gain and offset, the effects of pixel cross-talk and detector non-linearity, and the contributions of thermal radiation and stray-light are ignored in the current version (they will be included in future versions).

While the radiance spectrum of the observed light is simply obtained adding S_+ and S_-, the derivation of P and χ and especially their spectral resolution depends on the demodulation algorithm for a given set of optical components. For the demodulation of the measured, modulated radiance spectra S_+ and S_- (see Eq. 11) into spectra of P and χ, we use the technique outlined in [5]. This technique involves fitting of one or more periods of the local modulation. The fitting is applied on each 'spectral window' determined as:

$$\Delta\lambda = \frac{\lambda^2}{\delta(1 + \lambda^2/4\delta^2)}, \tag{13}$$

where $\Delta\lambda$ represents a spectral 'window' and δ is the retardance (see Eq.11) across that window. A spectral window covers a small wavelength region of the modulated radiance spectra across which P, χ, and the instrument's optical properties are assumed to be constant. Optimizing $\Delta\lambda$ means optimizing the sampling frequency and therefore, the spectral resolution of P and χ. Note that we

have not shown any spectra of χ; it is less sensitive to the atmospheric parameters than either I or P.

4.3. Simulated SPEX' observations

Here, we show the accuracy of the demodulation algorithm and its spectral resolution using simulated Titan spectra shown in Sect. 4 ($0^\circ \leq \theta_0 \leq 80^\circ$, $40^\circ \leq \theta \leq 90^\circ$, $\phi - \phi_0 = 0^\circ,\ 180^\circ$, and DLA- particles), in combination with the SPEX end-to-end simulator.

The spectral resolution depends mostly on the retardance. We will present results for different values of the retardance δ, starting with the value as chosen for SPEX on a Mars orbiter, namely $\delta \simeq 20$ μm (a crystal thickness of 4 mm), and then optimizing the value for SPEX on a Titan balloon. The main difference between these two missions would be the spectral resolution with which P is retrieved: while a Mars spectrum shows little to no spectral features across SPEX' wavelength region, a Titan spectrum is rich with methane absorption bands.

Figure 9 shows the retrieved P for the Mars-SPEX with $\delta \simeq 20$ μm and the retrieved P optimized for the Titan-SPEX, in which case $\delta \simeq 80$ μm. It also shows the errors in the retrieval, with our target error of at most 5 $\%$ (this error is based on retrieval algorithms for aerosol properties using polarization data [24]. With $\delta \simeq 20$ μm, the spectral resolution of P is about 8 nm in the blue and about 32 nm in the red (cf. Eq. 13). The top graphs in Fig. 9 show how arduous it is to fit the retrieved P to the original P. Clearly, this resolution is not good enough to resolve the methane band features.

In order to better resolve the methane band features[2], and to reach a retrieval accuracy within the target error, we have to increase the sampling frequency of the demodulation algorithm, hence to decrease the width of the spectral windows (cf. Eq. 13). This implies that we have to increase the retardance δ of our retarder, thus the thickness of the birefringent crystals (sticking with our choice of MgF_2-Al_2O_3 crystals). An optimal retrieval was found for a crystal thickness of 16 mm, four times as thick as in the original SPEX design (for a Mars mission), yielding a retardance $\delta \simeq 80$ μm. The optimized spectral resolution of the polarization spectra is 2 nm in the blue and 8 nm in the red. The spectrally improved retrieved P is shown at the bottom of Fig. 9 together with the error in the retrieval. Note that in the deepest parts of the methane bands, the error can still exceed our target error. If we want to use these parts to retrieve aerosol properties (see [8]), the instrument response has to be taken into account in the retrieval algorithm.

[2] An accurate retrieval of aerosol properties does not necessarily require complete resolving the methane bands, since the degraded resolution can be taken into account in the retrieval process. In general, however, the better the resolution, the more information can be retrieved

5. DESIGNING SPEX FOR A TITAN BALLOON

Here, we have presented SPEX's strengths as payload for the hot air balloon that is an intrinsic part of the Titan Saturn System Mission (TSSM). A detailed investigation of Titan's haze layer is key to expanding our the knowledge on the atmosphere's complex hydrocarbon cycle, which is one of the main goals of the TSSM. By measuring both the radiance and the degree of linear polarization of sunlight that has been scattered by the haze particles, SPEX allows the retrieval of the size, shape and composition of the haze particles and their vertical distribution. In addition, SPEX is small (about 1 liter volume), uses little power and its novel polarimetric technique requires no moving parts.

SPEX has originally been designed as payload for a Mars orbiter, with 7 fixed downward viewing and 2 fixed limb-viewing apertures, parallel to the orbiter's ground track. The main adaptations of SPEX to fly on a balloon mission through Titan's atmosphere would be the viewing geometries, and the spectral resolution. These will be discussed below.

5.1. Viewing geometries

The mission plan is to have the TSSM balloon float at a nominal altitude of 10 km with a range between 6 and 12 km. As payload on the balloon, the interesting viewing angles for SPEX are looking upwards, towards the haze layer, and possibly downwards, towards the surface. Knowledge of the surface reflection and its spectral and angular variations is important for understanding the formation and evolution of Titan, and for identifying possible sources and sinks of methane. And it is also crucial for understanding SPEX' observations of scattered sunlight, because direct and diffuse sunlight will be reflected off the surface, back towards the atmosphere, where it can undergo more scatterings. Hence, the surface reflection has to be included in the retrieval process.

Our numerical simulations have shown the importance of sampling I but especially P at various viewing angles, so we foresee to use either a number of apertures (as in the Mars design), with fixed viewing zenith angles distributed like a hand-fan between $\theta \approx 50^\circ$ and 130° (these angles would depend on the size of the balloon, the distance between SPEX and the balloon, and on the location of SPEX on the payload package), or a single aperture that scans up and down. SPEX should also be able to rotate in the horizontal plane to sample a range of azimuthal angles $\phi - \phi_0$. This rotating would be taken care of if the balloon payload would rotate (although the rotation period shouldn't be too long to avoid variations in the atmosphere). Better would be to have SPEX on top of the payload where it can rotate around a vertical axis, such as the connection between the payload and the balloon. Having SPEX below the payload would have the disadvantage of blocking the upward view.

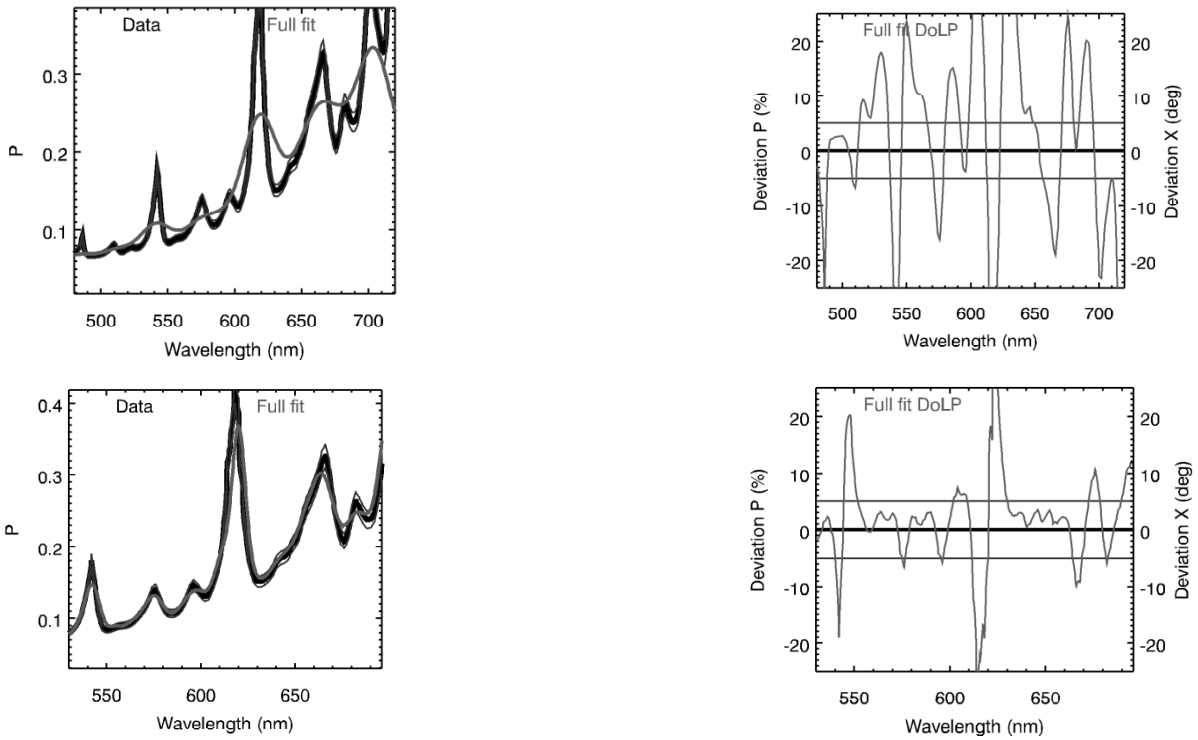

Figure 9. Retrieval of P using the demodulation algorithm of the SPEX end-to-end simulator: P (left) and the retrieval error with horizontal lines indicating a target error of at most 5 % (right). Two different values for the retardance δ of the multiple-order retarder were used: $\delta \simeq 20$ μm (top) and 80 μm (bottom). Note that 'DoLP' stands for 'Degree of Linear Polarization.'

An interesting solution that would allow the required angular sampling while limiting the number of moving elements, would be to have a rotating disk inclined under an angle of 40° with respect to the vertical axis, with a number of apertures looking outward along the rim of the disk.

5.2. Spectral resolution

SPEX has been designed to measure I, P, and χ from the visible to the near-infrared. Across this wavelength spectrum, a Mars spectrum does not show significant high-spectral resolution features. A Titan spectrum, however, is rich in methane absorption band features. Clearly, as also shown in Sect. 6, using the relatively low spectral resolution designed for the Mars-SPEX for the Titan-SPEX would result in too large errors in the retrieved values for P. To keep the errors in P below 5 %, we have to increase the retardance, hence the thickness of the birefringent crystals from the original 4 mm for Mars to 16 mm for Titan.

Increasing the retardance and hence the modulation frequency, requires an increase of the sampling of the modulated radiance spectra. To allow for a much higher sampling of the spectra, not only the detector size can be increased, but also the wavelength range that is covered. For a Titan-SPEX, a wavelength coverage from 0.5 to 0.72 μm could be considered. Such a wavelength range would have the additional advantage that it excludes the deep methane band at 0.73 μm, which is especially difficult to fit with our current demodulation algorithm. Adapted demodulation algorithms, e.g. algorithms that distinguish between the continuum and the methane bands, could be considered if the inclusion of this deep band is interesting for scientific reasons.

6. CONCLUSIONS

We have presented numerical simulations of the radiance and degree of linear polarization of sunlight that has been scattered in Titan's atmosphere, and of observations of this light as performed by the SPEX instrument as payload on the hot air balloon of the TSSM mission. In particular the degree of linear polarization of scattered sunlight is known to be very sensitive to the microphysical properties of the scattering particles. Floating in the atmosphere of Titan, SPEX novel spectropolarimetric technique would provide a valuable contribution to characterizing the famous hazes. Minor adaptations of the SPEX instrument as designed for placement on a Mars orbiter would be needed if SPEX were to fly on a Titan balloon: the viewing directions and the spectral range and spectral resolution. The latter is necessary to better resolve the methane absorption bands.

ACKNOWLEDGMENTS

We are grateful to dr. Y.V. Skorov, dr. S. Ramirez, dr. R. de Kok, and dr. M. Min for their help in developing our research.

REFERENCES

[1] Hansen J.E. and Travis L.D., Light scattering in planetary atmospheres, *Space Sci. Revs.*, **16**, 527-610, 1974.

[2] Aben I., Helderman F., Stam D. M., and Stammes P., Spectral fine-structure in the polarization of skylight, *Geophys. Res. Lett.*, **26**, 591-594, 1999.

[3] Waite Jr. J.H., et al. The process of tholin formation in Titan's upper atmosphere, *Science*, **316**, 870-875, 2007.

[4] Lunine J.I. and Atreya S.K., The methane cycle on Titan, *Nature Geoscience*, **1**, 159-164, 2008.

[5] Snik F., Karalidi T. and Keller C.U., Spectral modulation for full linear polarimetry, *Appl. Optics*, **48**, 1337-1346, 2009.

[6] Chandrasekhar S., Radiative transfer, *Oxford Univ. Press*, 1950.

[7] Hovenier J.W. and Van der Mee C.V.M., Fundamental relationships relevant to the transfer of polarized light in a scattering atmosphere, *Astron. Astrophys.*, **128**, 1-16, 1983.

[8] Stam D.M., De Haan J.F., Hovenier J.W., Stammes P., Degree of linear polarization of light emerging from the cloudless atmosphere in the oxygen A band, *J. Geophys. Res.*, **104**-D14, 16843-16858, 1999.

[9] De Haan J., Bosma P., Hovenier J., The adding method for multiple scattering calculations of polarized light, *Astron. Astrophys.*, **183**, 371-391, 1987.

[10] Flasar F.M. et al., Titan's atmospheric temperatures, winds, and composition, *Science*, **308**, 975, 2005.

[11] Ramirez S.I. et al., Complex refractive index of Titan's aerosol analogues in the 200-900 nm domain, *Icarus*, **156**, 515-529, 2002.

[12] McCord T.B. et al., Composition of Titan's surface from Cassini VIMS, *Planet. Space Sci.*, **54**, 1524-1539, 2006.

[13] Skorov Y.V., Keller H.U., Rodin A.V., Optical properties of aerosols in Titan's atmosphere, *Planet. Space Sci.*, **56**, 660-668, 2008.

[14] Tomasko M.G., Doose L.R., Dafoe L.E., See C., Limits on the size of aerosols from measurements of linear polarization in Titan's atmosphere, *Icarus*, **204**, 271-283, 2009.

[15] Mishchenko M.I., Travis L.D., Mackowski D.W., T-matrix computations of light scattering by nonspherical particles: a review., *J. Quant. Spectrosc. Radiat. Transfer*, **55**, 535-575, 1996.

[16] Tomasko M.G, et al., The Descent Imager/Spectral Radiometer Aboard Huygens , *Huygens: Science, Payload and Mission*, 1997.

[17] Tomasko M.G, et al., A model of Titan's aerosols based on measurements made inside the atmosphere, *Planet. Space Sci.*, **56**, 669-707, 2008.

[18] Karkoschka E., Spectrophotometry of the jovian planets and Titan at 300-to 1000-nm wavelength: The methane spectrum, *Icarus*, **111**, 174-192, 1994.

[19] Niemann H.B. et al., The abundances of constituents of Titan's atmosphere from the GCMS instrument on the Huygens probe, *Nature*, **438**, 779–784, 2005.

[20] Titan Saturn System Mission Study Final Report on the NASA Contribution to a Joint Mission with ESA, *Task Order NMO710851*, 30 January 2009.

[21] Mishchenko M.I., and Travis L.D., Satellite retrieval of aerosol properties over the ocean using measurements of reflected sunlight: Effect of instrumental errors and aerosol absorption, *Journal of Geophysical Research*, **102**-D12, 13543, American Geophysical Union 1997.

[22] Snik F., and Karalidi T., Trade-off study for the polarimetric principle of SPEX, *SRON private property*, 2008.

[23] Tishkovets V.P., Petrova E.V., Jockers K., Optical properties of aggregate particles comparable in size to the wavelength, *J. Quant. Spectrosc. Radiat. Transfer*, **86**, 241–265, 2004.

[24] Hasekamp O., and Landgraf J., Retrieval of aerosol properties over land surfaces: capabilities of multiple-viewing-angle intensity and polarization measurements, *Appl. Opt.*, **46**, 3332-3344, 2007.